

Understanding the dominant physics mechanisms on the p-i-n perovskite solar cells fabricated by scalable slot-die coating process in ambient air

Damian Glowienka[‡], Shih-Han Huang^{*‡}, Pei-Huan Lee*,
Feng-Yu Tsai*, Wei-Fang Su^{*‡§}

Perovskite solar cells (PSC) are emerging technologies that have shown continuous improvement in power conversion efficiency (PCE) and stability. However, a very important aspect that has been seldom considered is the reproducibility of PCE of PSC devices. It is possible to achieve PCE from 10.21% to 17.05% using scalable slot-die coating technique. However, a spatial distribution of performance is clearly observed for device samples on a 4 cm × 4 cm substrate. The relatively low PCE is mainly coming from the losses of electrical mechanism. In order to have in depth understanding of the losses, we used the dominant loss analysis techniques including numerical simulations to explore the mechanism. The results indicate part of efficiency decrease is due to the increase of bulk defect density which is linearly changed with the quality of the perovskite layer and related to recombination process. However, extremely high charge carrier transportation losses are found at the HTL/perovskite interface that are related to the Fermi level pinning mechanism for low efficiency device. The result of physics insight of perovskite solar cells has led to a strategy, where chemical passivation technique is used to achieve the PCE from 13.81% to 18.07% for the batch of devices with good reproducibility. This study reveals that the necessity to understand not only the champion device but look at all devices in different batches more broadly in order to improve the reliability of device fabrication process and to generate reproducible perovskite solar cells.

^{*}Department of Materials Science and Engineering, National Taiwan University, 10617, Taipei, Taiwan

[‡]Faculty of Applied Physics and Mathematics, Gdańsk University of Technology, Narutowicza 11/12, 80-233, Gdańsk, Poland

[‡]Department of Materials Engineering, MingChi University of Technology, 243303, New Taipei City, Taiwan

[§]corresponding author

1 Introduction

Perovskite solar cells (PSCs) became an emerging technology due to the highest growth in power conversion efficiency among the existing photovoltaic technologies [1, 2]. However, there are many challenges yet to be overcome to bring this technology from laboratory to commercialization. For instance, it requires development of large-area processing techniques that are compatible with industrial production [3]. There are a lot of reports focusing on manufacturing-worthy fabrication techniques of PSCs using the doctor blade [4, 5, 6], spray coating [7] and slot-die coating as alternatives to lab scale spin-coating. However, so far slot-die coating seems to be the most explored deposition method owing to its highly promising results [8].

Slot-die coating is well suited for the deposition of all layers in the device stack of PSCs. It is highly efficient in terms of materials usage as it yields a low wastage of inks [8]. In the regular slot-die coating process, a coating head is placed close to a substrate. An ink is pumped into the coating head using a syringe pump to form a liquid layer on the substrate. The substrate is moved along the head to make the deposition of a wet film. The thickness of the wet film deposited is controlled by adjusting the flow of ink and the speed at which the substrate moves. This allows for very fine control of the film thickness after drying from a few of nm to tens of microns simply by adjusting the ink flow rate or substrate speed [9].

The drying process is a very critical part that impacts the quality of the perovskite layer, with many available options including quenching with a nitrogen flow or in vacuum, by contact heating, by radiation heating, and combinations of these individual options. We have previously demonstrated a drying process utilizing rapid near-infrared radiation heating in ambient air [10], which produced high-quality films on a large area of 12 cm \times 12 cm. Even though it seems to be much preferable technique comparing to hot-plate, there is still space for improvement by the meaning of the layer quality. Especially, that the technique is very sensitive for processing parameters and the choice of substrate, when forming the perovskite layer. It is vital to have defect free perovskite film with large grain size, crystal phase purity and good film coverage that can deliver higher photovoltaic performance and stability [11]. It is often visible in the champion device performance, but the most importantly is the statistical distribution of the device performance. From the commercialization point of view, it is imperative to fabricate devices reproducibility with ease to have a low product cost. Researches are focusing mostly on the champion devices; the reproducibility of the devices has not been studied so far and thus neglecting middle or low efficiency samples. However, to improve the reproducibility of the PSCs, a better understanding is necessary. Here, we try to find the dominant loss mechanisms of PCE distribution within one batch and different batches in slot die coating process. The results can create strategy of process optimization to narrow down the PCE distribution and improve the average PCE performance for each batch. We propose the passivation with the 2-thiophene ethylammonium chloride (TEACl) on the top of the absorber layer to improve

the later and interface quality [12]. Hsiao et al. show that TEACl passivation can not only improve the PCE but also increase the stability of the PSCs.

2 Results and Discussion

The standard perovskite solar cells (PSCs) were prepared using a slot-die coating process. The devices were prepared in the opaque p-i-n stack with glass/FTO/NiO_x/P3HT-COOH/perovskite/PCBM/PEI/Ag configuration. The layers of NiO_x, P3HT-COOH and perovskite were fabricated using slot-die, the layers of PCBM and PEI using spin-coating and Ag electrode using thermal evaporator. Using the profilometer and optical measurement techniques, the thickness of each layer in the stack was measured separately: NiO_x is 61±3 nm, P3HT-COOH is 5±1 nm, perovskite absorber layer is 450±22 nm, PCBM is 40±2 nm and Ag is 100±1 nm. The error accounts mostly for the roughness and nonuniformity of the films. It is especially visible in the SEM cross-section image, see Figure S1A (Supplementary Information). The sample has been made on 4×4 cm substrates and cut into smaller size of 2×2 cm substrates before the deposition of PCBM and PEI layer. On each sample, 6 fully operable perovskite solar cells were made. Therefore, 24 devices were prepared on every 4×4 cm substrate, as shown in Figure S1B (Supplementary Information). The perovskite layer uniformity has the greatest impact on the performance of the PSCs. Therefore, we have additionally measured the thickness of the absorber layer on each of the 2×2 cm substrates. The samples have shown the variation of 9.7 nm which accounts for the error of around 2%.

The device performance has been analyzed with J(V) measurement under AM1.5G light illumination. Figure 1 shows the distribution of power conversion efficiency (PCE) of devices on 4×4 cm substrate. The efficiency of the devices is ranged from 0% to 17.70%. We also prepared additional two batches with the same device configuration, see Figure S2 and S3 (Supplementary Information). In total, we measured 72 devices. The devices from the first batch shows the lowest efficiency device located in the middle of the 4×4 cm substrate (Figure 1A). Similar nonhomogeneous behavior is observed for the devices in the other batches, as shown in Figure S2A and S3A (Supplementary Information). There are multiple reasons to explain the low repeatability of the PSCs. In order to improve the process, we need better understanding of the dominant mechanisms taking place in the devices exhibiting in high to low PCE.

Figure 1B-E shows the results of statistical distribution of performance of 24 devices on the same substrate. The PCE of all devices give an average 14.62±1.18%, see Figure 1B. The fully shunted devices with zero efficiency are not included in the graphs. The other two batches gave the average results equal to 13.66±2.62% and 12.68±2.88%, as shown in Figure S2B and S3B (Supplementary Information), respectively. The variation of short-circuit photocurrent (J_{sc}) is rather small and equal to 19.94±0.59 mA cm⁻² (Figure 1C). The other two batches are showing slightly lower J_{sc} that is equal to 18.74±2.25 mA cm⁻² and 18.31±2.31 mA cm⁻² (Figure S2C and S3C in Supplementary Informa-



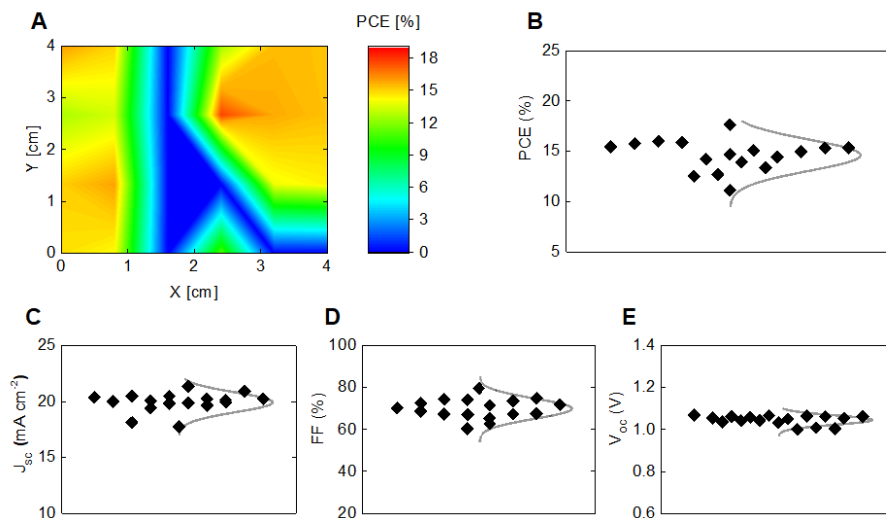


Figure 1: A) Spatial distribution, B) PCE, C) J_{sc} , D) FF, and E) V_{oc} results for the reverse scan measurement perovskite solar cells obtained from one 4 cm \times 4 cm substrate.

tion), respectively. Figure 1D shows the fill-factor (FF) distribution is equal to $69.97 \pm 3.88\%$ for the first substrate. The other two substrates exhibit FF that varies within $73.49 \pm 5.58\%$ and $70.37 \pm 5.48\%$ (Figure S2D and S3D in Supplementary Information), respectively. Lastly, the open-circuit voltage (V_{oc}) is equal to 1.05 ± 0.02 V, 0.97 ± 0.05 V and 0.96 ± 0.07 V for Figure 1E, S2E and S3E (Supplementary Information), respectively. Considering the distribution of all devices within three substrates, we clearly see that the PCE of majority devices are in a wide range from 5% to 17%. By analyzing just one representative device would not give full picture on the mechanisms controlling with such wide distribution. Also, the statistical variation is clearly observable among three substrates. Therefore, we have decided to pick three representative devices with PCE equal to 17.05%, 15.33% and 10.21%. They were further analyzed in detail to understand what are the main factors influencing the wide distribution of PCE performance of devices. We called the devices high, intermediate and low, respectively. Also, the devices were chosen from the first batch, thus eliminating the batch variation to simplify the study.

In order to determine the dominant mechanism that limits the device performance, the three chosen devices were firstly assessed with short time stability under maximum power point tracking (MPPT) procedure [13]. Figure S4A (Supplementary Information) shows the MPPT measurements for high, intermediate and low PCE devices. Both, high and intermediate devices exhibit very stable MPP under 2 minutes measurement. Most of the devices in single

1 batch are usually similarly stable and only small drop or rise is observed in the
 2 very first few seconds of the measurements. However, some of the devices are
 3 dropping down very quickly, which made it much harder to define the dominant
 4 mechanism since more precise measurements are necessary. For that reason,
 5 we measured $J(V)$ characteristics under AM1.5G conditions before and after
 6 full electrical characterization, see Figure S4B–D (Supplementary Information).
 7 The full characterization means the MPPT and $J(V)$ measurements with neutral
 8 density (ND) filters according to the protocol mentioned in the Experimental
 9 Section. It is clearly visible that for high PCE device, the $J(V)$ characteristics
 10 does not change throughout the measurements (Figure S4B, Supplementary In-
 11 formation). Small drop in V_{oc} and FF is observed for the intermediate sample
 12 (Figure S4C, Supplementary Information). This effect could be attributed to
 13 slow degradation of the sample under continuous light soaking, where the PCE is
 14 slowly decreasing [12]. The tremendous effect is observed on the low PCE sam-
 15 ple (Figure S4D, Supplementary Information). The device with low efficiency
 16 very often exhibits low stability in general. Also the visible drop of V_{oc} and
 17 FF is observed together with flattening of $J(V)$ curve above open-circuit (OC)
 18 conditions. In this case, we observe S-shape behavior before and after electrical
 19 characterization [14]. The S-shape is the characteristic flattening of the $J(V)$
 20 curve above OC region that usually appears, when the transport properties of
 21 the layer are very poor so it starts to behave like an insulator. This effect is
 22 very often reversible and after keeping in the dark it appears to disappear [15].
 23 Therefore, the precision of the analysis is decreasing due to instability of the
 24 sample during the measurements. For most of the cases, we observe that the dis-
 25 tribution of PCE of device samples are limited by their FF and V_{oc} . J_{sc} appears
 26 to be the least statistically distributed among the samples and its loss is only
 27 visible for low PCE sample. To validate it, we measured External Quantum
 28 Efficiency (EQE) of the three representative samples (Figure S5, Supplemen-
 29 tary Information). The calculated J_{sc} values are equal to 19.43 mA cm^{-2} , 19.16
 30 mA cm^{-2} and 19.04 mA cm^{-2} for high, intermediate and low PCE devices,
 31 respectively. Meaning, the J_{sc} loss should not lead to the drop of %PCE more
 32 than 0.5%. Therefore, the observed losses are rather attributed to the electrical
 33 losses than optical one. Especially that for low PCE sample, the J_{sc} difference
 34 between measurements of EQE and $J(V)$ is around 2.4 mA cm^{-2} . The reason is
 35 that under EQE measurement, its monochromatic light generates low amount of
 36 charge carriers which makes the interface mechanism hardly observable. Thus,
 37 we focused only on the electrical mechanism that dominates the performance of
 38 the PSCs.

39 Before we investigated further for the dominant loss mechanism of trans-
 40 portation and recombination of charge carriers, we briefly analyzed the gen-
 41 eral losses from Shockley–Queisser (SQ) model of solar cells from Equation (1)
 42 [16, 17].

$$\frac{\eta_{real}}{\eta_{SQ}} = F_{FF}^{res} \frac{FF_0 (V_{oc}^{real})}{FF_0 (V_{oc}^{SQ})} \frac{V_{oc}^{rad}}{V_{oc}^{SQ}} \frac{V_{oc}^{real}}{V_{oc}^{rad}} \frac{J_{sc}^{real}}{J_{sc}^{SQ}} \quad (1)$$

1 Where η_{real} and η_{SQ} are two efficiencies of real device and SQ theoretical
 2 device, respectively. F_{FF}^{res} is equal to $FF_{real}/FF_0(V_{oc}^{real})$, where FF_{real} is ex-
 3 perimentally measured FF of the solar cell and FF_0 represents FF value without
 4 resistive losses at given V_{oc} calculated using diode equation. V_{oc}^{real} , V_{oc}^{rad} and
 5 V_{oc}^{SQ} represents open-circuit voltage of real solar cell, ideal device with only ra-
 6 diative losses and with SQ limits, respectively. J_{sc}^{real} and J_{sc}^{SQ} are short-circuit
 7 current measured experimentally and idealized form SQ model, respectively.
 8 The results of calculation based on the characteristics of EQE and J(V) and the
 9 equations are shown in below. Three band-gaps are equal to 1.606 eV, 1.606 eV
 10 and 1.598 eV for high, intermediate and low PCE samples from the EQE mea-
 11 surements, respectively. The decreased band-gap for low PCE sample may be
 12 due to high defect concentration in the shallow levels [18]. Therefore, for a de-
 13 vice of 1.606 eV band gap, the theoretical Shockley–Quisser limit for V_{oc} , FF,
 14 J_{sc} and PCE are equal to 1.333 V, 90.60%, 25.32 mA cm⁻² and 30.57%, respec-
 15 tively. The PCE losses in respect to Shockley–Quisser limit are calculated for
 16 high, intermediate and low PCE samples, as shown in Figure S6 (Supplemen-
 17 tary Information). The total efficiency is normalized to represent 100% and
 18 can be attributed to the losses of FF, V_{oc} and J_{sc} in respect to SQ model.
 19 Firstly, the loss of FF can be attributed to the transportation loss of charge
 20 carriers including parasitic resistance (F_{FF}^{res}) and nonradiative recombination
 21 ($FF_0(V_{oc}^{real})/FF_0(V_{oc}^{SQ})$), see Equation 1. All the devices were made with
 22 the same configuration and geometry of the electrodes; therefore, we expect no
 23 difference in the loss of series resistance of three devices. Thus, the F_{FF}^{res} can
 24 be attributed to the transportation loss which is the major factor contributing
 25 to the total loss of the efficiency. The transportation losses of three samples
 26 are equal to 8%, 14% and 27% for high, intermediate and low PCE samples,
 27 respectively. In general, any loss mechanism of charge carriers that leads to the
 28 drop of PCE can be attributed. To seek the clarity in our analysis, we only con-
 29 sidered possible changes in charge carrier mobility, energy band alignment and
 30 tunneling process between the transportation and absorption layers. However,
 31 the presence of an additional buffer layers would also change the charge carrier
 32 loss mechanism due to the transportation mechanism. The loss of FF is also
 33 related to nonradiative recombination $FF_0(V_{oc}^{real})/FF_0(V_{oc}^{SQ})$ which depends
 34 on the quality of device samples. High, intermediate and low PCE samples are
 35 having losses equal to 6%, 8% and 10%, respectively. The loss of V_{oc} is due to
 36 two parameters (1) nonideal shape of quantum efficiency (V_{oc}^{rad}/V_{oc}^{SQ}) and (2)
 37 nonradiative recombination ($V_{oc}^{real}/V_{oc}^{rad}$). The first one is approximately the
 38 same for all three samples and equal to 1%. The second one is equal to 17%,
 39 16% and 16% for high, intermediate and low PCE solar cells, respectively. From
 40 this simple Shockley–Quisser model we can observe that the trap recombination
 41 is not main factor influencing the V_{oc} loss. The losses of J_{sc} for high, intermedi-
 42 ate and low samples are equal to 15%, 14% and 11% respectively which is from
 43 the optical parasitic absorption losses ($J_{sc}^{real}/J_{sc}^{SQ}$) and related to the quality of
 44 the sample. Since J_{sc} is decreasing with the reverse order of the device quality,
 45 we expect that the photocurrent loss is due to electrical mechanisms, not the

optical. The J_{sc} stays in agreement with the EQE shapes for all three samples with negligible differences. At last, the samples are reaching 53%, 47% and 35% of the Shockley–Quisser limit with respect to their measured PCE. Therefore, our focus in the next analysis was concentrated on the electrical mechanism of PCE loss that is related to transportation and nonradiative recombination.

We used modulated light intensity technique by measuring the $J(V)$ characteristics under different AM1.5G light concentration then compared the results with simulation using electrical drift–diffusion model [19]. Figure S7 (Supplementary Information) shows $J(V)$ characteristics for experimental and simulated curves under 6 light intensities. The modulated light intensity was calibrated before all the measurements with the filters with a decreasing order of 1.0000 ± 0.0000 , 0.5287 ± 0.0038 , 0.2739 ± 0.0015 , 0.1220 ± 0.0008 , 0.0240 ± 0.0013 and 0.0095 ± 0.0025 . The values are calculated based on the ratio of J_{sc} with and without ND filter of all the measured PSCs. Therefore, the error of measurement is also calculated by standard deviation and it is increasing linearly with lowering of light intensity as follows 0.00%, 0.72%, 0.54%, 0.66%, 5.28% and 25.86%, respectively. Thus we defined them as 1 sun, 0.5 sun, 0.3 sun, 0.1 sun, 0.02 sun and 0.01 sun, respectively. The simulation parameters are given in Table 1. The goodness-of-fit is equal to 98.9% for all points that indicates a very good correlation between the model and experimental data; not only below OC (open-circuit), but also above OC for all $J(V)$ characteristics. The $J(V)$ results reveal the generation and recombination mechanisms, but also it describes well the dominant mechanism of charge transportation for simulated devices.

It is much easier to interpret the modulated light intensity analysis using photovoltaic parameters (PCE, J_{sc} , FF and V_{oc}) that gives all necessary details of $J(V)$ characteristic (Figure 2). The PCE was calculated by varying the input power which is related to the light intensity (Figure 2A). The PCE was increased with the light intensity linearly and reached maximum at the highest light intensity. Figure 2B shows the J_{sc} that is almost a linear function of light intensity with an alpha being very close to 1 from semi-log plot. Alpha parameter describes the linearity of J_{sc} in function of light intensity in the short-circuit (SC) region of applied voltage. Therefore, if alpha is close to 1 or to 2, it means the monomolecular (trap assisted) recombination or bimolecular (radiative) recombination is the dominant recombination mechanism, respectively. The relationship between FF and light intensity shows recombination and transportation loss simultaneously (Figure 2C). Firstly, the peak value of FF (peak-FF) appears at around 0.1 suns and it is equal to 79.74%. Considering the Shockley–Quisser limit of solar cell with a band-gap of 1.606 eV, we would expect the FF at the level of 90% independently on the light intensity. In the case of peak-FF, the loss comes mainly from the bulk defect recombination of charge carriers [20]. Therefore, the loss of 10% is due to intermediate defects in the bulk of perovskite layer. High crystallinity of bulk is desired to reduce the effect of the bulk defect recombination on the peak-FF value. At 1 sun, the FF is equal to 77.96% which shows 2% drop in respect to peak-FF. This means interface loss is present in high PCE sample. To complete the picture of recombination ratio between interface and bulk we might use V_{oc} as a function of light

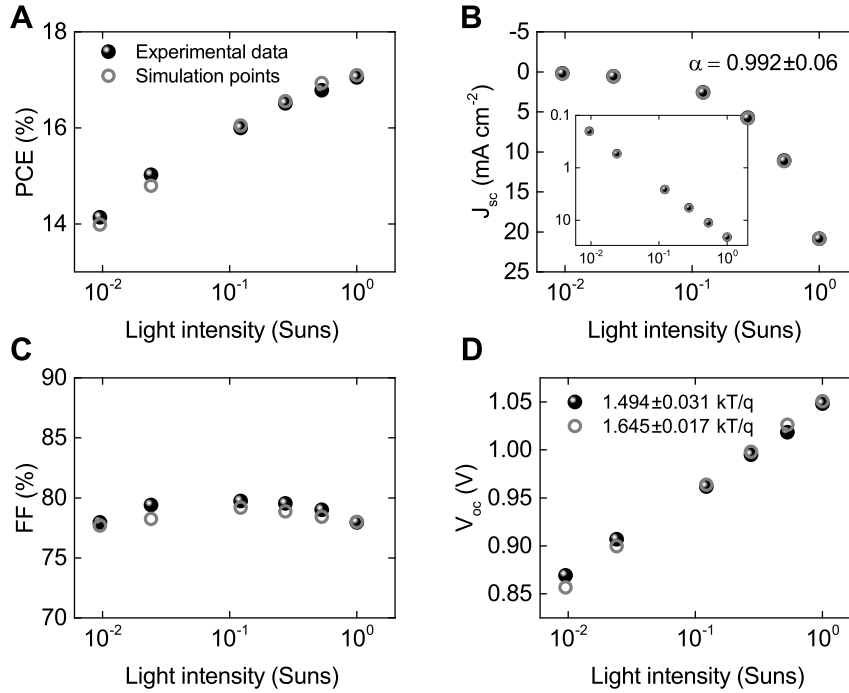


Figure 2: Experimental and simulation results of A) PCE, B) J_{sc} , C) FF, and D) V_{oc} results for the reverse scan measurement of high PCE perovskite solar cell.

1 intensity in semi-log plot (Figure 2D). V_{oc} at 1 sun and the ideality factor [21]
2 of the high PCE device are equal to 1.048 V and 1.494 ± 0.031 kT/q, respectively.
3 The Shockley–Quisser limit for the band-gap of 1.606 eV is equal to 1.333 V,
4 thus 285 mV is being lost due to the recombination process. We speculate the
5 losses are from the recombination process at the interface and in the bulk. The
6 drift-diffusion model of device was used to get insight of recombination process
7 [22].

8 The simulation parameters and fitted parameters are shown in Table 1 of
9 simulation section. A very good match between simulation and experimental
10 results for the device samples. Table 1(a) shows general parameters used for
11 high, intermediate and low PCE devices. These parameters are all fixed and
12 extracted from either experiment or literature. All the samples exhibit low series
13 and shunt resistance losses and good energy alignment between HTL, ETL
14 and absorber if considering Shockley transport between the layers. Also, perovskite
15 layer has shown high mobility of charge carriers which would be related
16 to the very good crystallinity of the layer and positively affect the efficiency of
17 the devices. This is well matching a very good PSC with long diffusion length
18 that lead to high performance of solar energy conversion [31]. In Table 1(b)

Table 1: List of parameters used in the simulation of the PSCs. Parameters for holes in bracket and electrons without bracket. Also, values taken from the literature are given with their references.

(a) Parameters used in the simulation for each layer in the solar cell.

	Name	Unit	NiOx/P3HT-COOH	perovskite	PCBM
L	Thickness	nm	61	450	37.5
ε	Permittivity		2.1	24.1 [23]	3.75
$\mu_{n(p)}$	Mobility	$\text{cm}^2 \text{V}^{-1} \text{s}^{-1}$	(0.01) [24]	16.35 (16.35)	0.002 [25]
$C_{n(p)}$	Capture rate	$10^{-14} \text{m}^3 \text{s}^{-1}$	-	1 (1)	-
$\gamma_{n(p)}$	Auger coefficient	$10^{-40} \text{m}^6 \text{s}^{-1}$	-	1.55 (1.55) [26]	-
ζ	Langevin prefactor		-	1.2×10^{-5}	-
$E_{c(\nu)}$	Energy level	eV	(-5.4149)	-3.88 (-5.46) [27]	-3.90 [28]
$N_{D(A)}$	Doping concentration	m^{-3}	(1.21×10^{21}) [24, 29]	(1×10^{19}) [30]	0
$N_{c(\nu)}$	Effective density of states	m^{-3}	2.5×10^{25}	10^{24} [28]	2.5×10^{25}
R_s	Series resistance	Ωcm^2		0.1	
R_{sh}	Shunt resistance	$10^6 \Omega \text{cm}^2$		1.1×10^6	

(b) Fitted parameters from the simulation of PSCs for high, intermediate and low PCE devices for the trap densities.

	Name	Unit	High	Intermediate	Low	TEACI
$N_{tn(p)}$	Bulk trap density	10^{22}m^{-3}	1.17 (1.17)	2.54 (2.54)	17.77 (17.77)	1.08 (1.08)
	HTL interface trap density	10^{14}m^{-2}	(49.86)	(50.00)	(22.37)	(41.25)
	ETL interface trap density	10^{14}m^{-2}	31.36	31.43	8.30	50.41
	Band-bending	10^{14}m^{-2}	0	77.6	261.1	0
	Ratio of mobility at the interface	10^{14}m^{-2}	1	14414	1256	1

we can find the fitted values from the model through the best fit of the experimental data. For high efficiency device, the bulk trap defect density is equal to $1.17 \times 10^{22} \text{m}^{-3}$ which could be considered as relatively high from device point of view. However, we did not observe the extremely high V_{oc} and FF losses which are mostly due to very good mobility of charge carriers in the absorber layer. Thus, the loss recombination in the bulk is lowered. At the same time, we have found HTL/perovskite and perovskite/ETL interface trap densities are equal to $49.86 \times 10^{14} \text{m}^{-2}$ and $31.36 \times 10^{14} \text{m}^{-2}$, respectively. These high values might lead to observable losses of V_{oc} and FF at high light intensities. All the values are fitted with maximum error of 0.3%. It is rather hard to distinguish whether HTL/perovskite or perovskite/ETL interface is dominating the opaque devices, where both interfaces exhibit similar recombination process [19]. There are cases, when high asymmetry of charge carriers is clearly visible and we might find which interface exhibit the dominant recombination. It is only possible when applying more conditions with different temperature, bias, light intensity or bifacially of solar cell. No additional mechanisms can be found from the modeling of the high PCE sample. Therefore, the losses are dominated by the recombinations at interfaces and in the bulk of perovskite which lead to a loss of peak-FF, slight drop in FF at high light intensity and total loss of 285 mV V_{oc} at 1 sun. They affect the ideality factor to be very close to 1.5 kT/q . We used this high PCE device sample as a reference for the

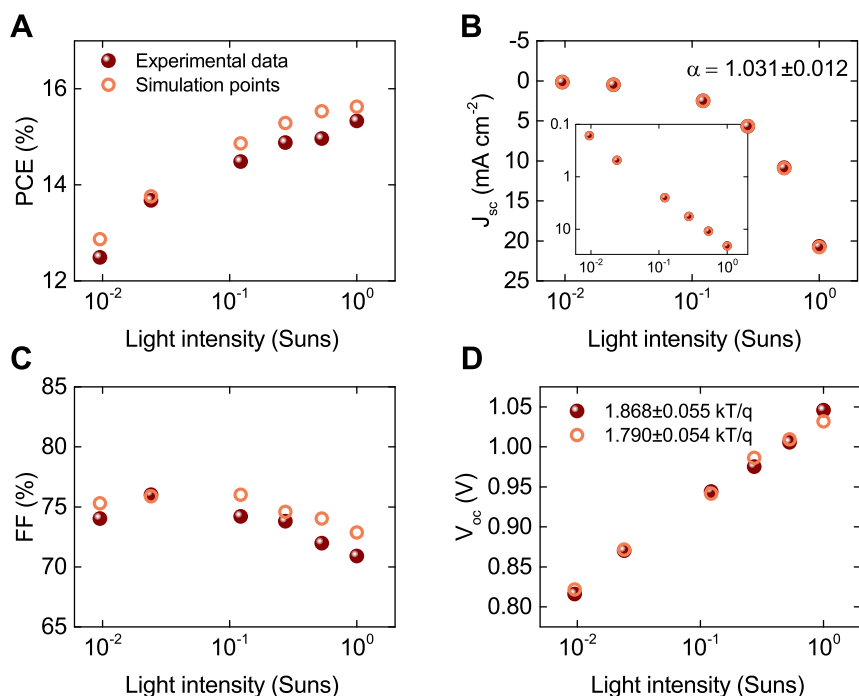


Figure 3: Experimental and simulation results of A) PCE, B) J_{sc} , C) FF, and D) V_{oc} results for the reverse scan measurement of intermediate PCE perovskite solar cells.

1 next analysis of intermediate and low PCE devices.
2 Here, we focused on the intermediate PCE device. This level of efficiency is
3 statistically the most often acquired from the batch if considering the normal
4 distribution of all samples. Figure S8 (Supplementary Information) shows $J(V)$
5 characteristics for experimental and simulated curves under modulated light
6 intensities. The goodness-of-fit is equal to 99.62% for all points in the charac-
7 teristics. We can clearly see that the slope of the region above OC has a lower
8 slope as compared with the high PCE device. The result indicates the interme-
9 diate device has possible issues with the transportation of free charge carriers.
10 The slope is clearly decreased with lowering of the light intensity. This observa-
11 tion is a very important point in the upcoming discussion of both intermediate
12 and low efficiency PSCs.
13 Figure 3 shows the experimental and simulation results of PV parameters
14 for intermediate PCE sample. The PCE of device exhibits a decreasing trend as
15 a function of light intensity with a small flattening at around 1 sun (Figure 3A).
16 Figure 3B shows the relationship of J_{sc} to the light intensity. The linear rela-
17 tionship with an alpha of 1.031 ± 0.012 reveals the trap assisted recombination
18 is a dominant process under short circuit conditions (SC). The alpha will in-

crease to 2.00 by improving the device quality to have only dominate radiative recombination. As compared with high efficiency PSC, the value is in the lowest possible region. The peak-FF is slightly moved toward 0.01 suns with a value of 76.02% (Figure 3C). These two observations are extremely important to understand the device operation in depth, not only the intermediate PCE device, but also the performance distribution of device samples in the slot-die coated substrate. Firstly, the down-shift of the peak-FF as a function of light intensity suggests that the shape of the whole FF is changed. This is mostly due to the loss of FF at 1 sun that is equal to 70.91%. Meaning, the interface issue is starting to appear and become very visible at higher light intensities. Secondly, the lowered peak-FF means that the bulk defect density is increased or the bulk crystallinity of perovskite is poorer and it leads to higher transportation loss of charge carriers in the bulk. These two processes can be separated in the relationship of V_{oc} as a function of light intensity (Figure 3D). In principle V_{oc} at 1 sun is equal to 1.046 V, meaning that it has dropped negligibly if comparing to high PCE device. Thus, the interface issues are closely related to the transport losses rather than the increase of interfacial defect concentration. However, the ideality factor is equal to 1.868 ± 0.055 kT/q which also means that V_{oc} at lower light intensity has dropped more significantly. This clearly suggest that the bulk recombination is lowering both peak-FF and V_{oc} at the same time. The transportation issue in the bulk could not lead to such a significant loss in the V_{oc} at a lower light intensity.

Figure 3A shows there is a small mismatch in high light intensity from the simulation results PCE as a function of light intensity. However, this parameter was calculated based on all PV parameters and the difference is lower than 0.5%. We can also clearly see that the bulk defect density is increased almost twice to a value of $2.54 \times 10^{22} \text{ m}^{-3}$ as compared with high PCE sample (Table 1(b)). Both samples have the same HTL and ETL interfaces. Therefore, all stays in agreement with the previous qualitative analysis. However, the energy levels of conduction and valence bands in the intermediate PCE sample could not be simply explained with the flat energy levels. The Fermi level pinning has been reported in the HTL/perovskite interface [32]. In order to get a high quality fit of the experimental data, the small band-bending of the energy levels was applied at the interface between HTL and perovskite absorber layer. We were able to simulate this effect by using few nanometers of perovskite layer with down-shifted conduction and valence bands. The total energy shift for the intermediate efficiency PSC is equal to 77.6 meV as compared with high PCE device. However, at the interface, there is a certain drop of mobility which lowers the transport of charge carriers by around three orders of magnitude if comparing to the mobility of perovskite layer (Table 1(a)). The mobility of the interface is around $10^{-3} \text{ cm}^2 \text{ V}^{-1} \text{ s}^{-1}$ which is in the range of organic layers. Therefore, the accumulation of charge carriers is present together with band-bending process. We tried to use other transport mechanisms at both interfaces in order to explain the phenomena of lowering of the J(V) slope with lowering of the light intensity, a very small drop of V_{oc} at 1 sun, and a large drop of FF at high light intensity from the experiments. However, the best results are



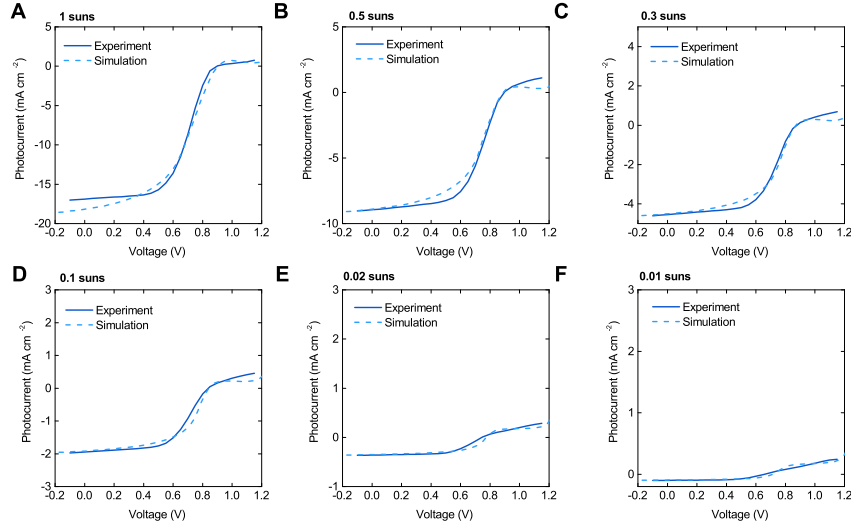


Figure 4: Experimental and simulation results of the $J(V)$ characteristics for low PCE sample under A) 1 sun, B) 0.5 suns, C) 0.3 suns, D) 0.1 suns, E) 0.01 suns, and F) 0.001 suns light illumination.

1 obtained with band-bending effect at the HTL/perovskite interface. Therefore,
 2 we conclude the performance losses of slot die fabricated device are mainly from
 3 the proposed transportation loss mechanism of charge carriers.

4 Figure 4 shows $J(V)$ characteristics for low efficiency PSC with experimental
 5 and simulated curves under modulated light intensities. The goodness-of-fit is
 6 equal to 91.15% for all points in the characteristics which is the lowest quality fit
 7 of the experimental data with the theoretical model. However, at the same time
 8 we can clearly see it is the most challenging one to explain. The reason is that
 9 there is a certain drop of slope of $J(V)$ characteristics in both regions of the SC
 10 and OC. Also, there appears S-shape in the region above OC conditions [33].
 11 We can also observe that the slope of the S-shape decreases with decreasing
 12 light intensity which is the same effect observed in the intermediate efficiency
 13 PSC.

14 Figure 5 shows the experimental and simulation results of the low perfor-
 15 mance PSC. The PCE of the device is flattening at high light intensity with a
 16 small drop at 1 sun (Figure 5A). The highest value of PCE appears at 0.5 suns
 17 at 9.28%. This kind loss clearly suggests the interface issues occur at high light
 18 illumination. A good linear relationship of 1.088 ± 0.032 between J_{sc} and light
 19 intensity is again observed (Figure 5B). The peak-FF of 58.71% is reached at
 20 10^{-2} suns but probably it would be at lower light intensity if we measure in a
 21 wider range (Figure 5C). The result indicates there are huge recombination loss
 22 in bulk or transport loss of free charge carriers. In the high range of light inten-

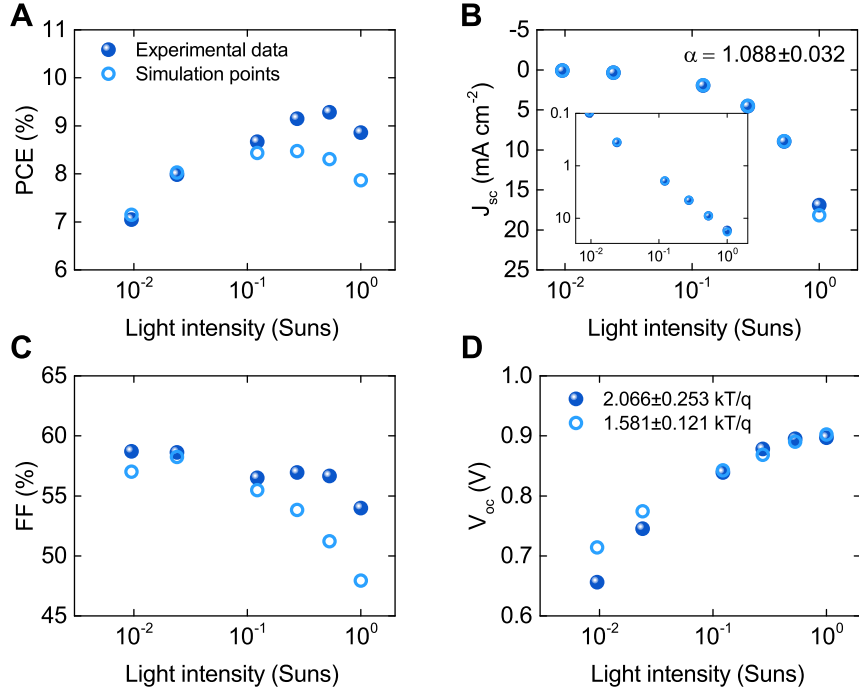


Figure 5: Experimental and simulation results of A) PCE, B) J_{sc} , C) FF, and D) V_{oc} results for the reverse scan measurement of low PCE perovskite solar cells.

1 sity, we clearly observe a nonlinear drop of FF which reaches the lowest value of
 2 to 53.98% at 1 sun. Therefore, the drop of FF is equal to around 5% between
 3 the peak-FF and FF at 1 sun. The mechanism responsible for such a drop in FF
 4 is well recognized with interface issues [19]. Further analysis of the simulation
 5 results will reveal more details whether it is related to the transport or recombi-
 6 nation mechanism. Figure 5D shows a highly nonlinear behavior relationship of
 7 V_{oc} as a function of light intensity which is clearly different from that of other
 8 two devices. At 1 sun open circuit voltage, the V_{oc} is equal to 897 mV which
 9 gives a loss of 436 mV as comparing to the limit of Shockley–Queisser model.
 10 The V_{oc} was dropped further at low light intensity which changed the ideality
 11 factor to 2.066 ± 0.253 kT/q. Also, the flattening at 1 sun is observed which is
 12 directly related to the losses at the interface [34]. The calculated two ideality
 13 factors are 1.096 ± 0.293 kT/q from 1 sun to 0.1 suns and 2.764 ± 0.399 kT/q from
 14 0.1 suns to 0.01 suns. The result shows a high nonlinearity of V_{oc} as a function
 15 of light intensity. At high light intensity, the dominant process is shown to be
 16 related to the interface recombination from the results of very low ideality factor
 17 and high FF losses at the same time. At lower light intensity, the nonradiative
 18 bulk recombination appears to be the dominant mechanism and it matches the

1 loss of peak-FF.

2 In addition to the qualitative analysis of the low efficiency PSC, we can make
3 quantitative analysis based on the simulation results as shown in Figure 5. The
4 match between the results of experiments and simulation is very poor at high
5 light intensity. It is mostly due to FF mismatch at high light illumination. The
6 steady-state drift-diffusion model [35] is not considering the time evolution of
7 $J(V)$ characteristics. However, as we point out before, the samples with low
8 PCE are less stable with time. They need either a longer time to stabilize or
9 their performance changes during the operation. Therefore, considering this in-
10 stability and also the appearance of S-shape in $J(V)$ characteristics, we assume
11 the model in steady-state conditions is not able to match with the experimental
12 results any better. Table 1(b) shows the fitting parameters from the modulated
13 light intensity simulation results. The bulk defect density of low performance
14 PSC is about 17 times of that of high performance PSC ($17.77 \times 10^{22} \text{ m}^{-3}$ vs.
15 $1.17 \times 10^{22} \text{ m}^{-3}$). This result indicates the charges recombination in bulk is
16 dominating factor to determine the performance of device prepared using the
17 slot-die coating process. On the other hand, the recombinations from HTL
18 and ETL interface defects are decreased as compared with to those of high or
19 intermediate PSCs. This can be explained considering that the bulk and inter-
20 face defects are part of the same nonuniform distribution. Therefore, since the
21 bulk defect concentration has increased so much, it might numerically appear
22 as an improvement of both interfaces. Sherkar et al. shows similar behavior
23 [28], where asymmetrical interfaces are appearing as bulk recombination itself.
24 The simulation shows the low PCE device exhibits a large Fermi level pinning
25 of 261.1 meV (band-bending) at the HTL/perovskite interface. This is at least
26 three times higher than for the intermediate device (77.6 meV). We have also
27 found out that the charge carriers at this interface are 1256 slower than in the
28 perovskite layer. Higher band-bending will stop the charge carriers from be-
29 ing transported but carrier mobility will affect its collection effectiveness. The
30 decrease of charge carrier concentration at the HTL can be described with Schot-
31 tky model $p = N_v \exp(-\phi_{HTL}/(k_B T))$, where maximum hole concentration is
32 described by the effective density of states in the valence band (N_v) and due to
33 the extraction barrier (ϕ_{HTL}) part of charge carriers are not able to cross the
34 energy barrier due to too low energy and might lead to their trapping in the
35 energetical quantum well, see Figure 6. Based on the Schottky model, for the
36 case of low PCE sample, where the energy barrier is equal to around 261 meV,
37 it gives 0.004% of free charge carriers that would be able to escape from the en-
38 ergetical trap, see Figure 6 (inset). Therefore, more than 99% of charge carriers
39 are stuck at the interface and they would recombine over time which would lower
40 the performance of the PSC. This also means that the carrier mobility at the
41 interface layer does not affect too much anymore due to few charge carriers to
42 be influenced. Also, the interface recombination highly depends on the amount
43 of free charge carriers being transported by the interface. Therefore, high dif-
44 ference in the energy levels between the layers leads to slower transport at the
45 interface and higher accumulation of charge carriers. Meaning, if more charge
46 carriers are present at the interlayer, the probability of their loss increases due

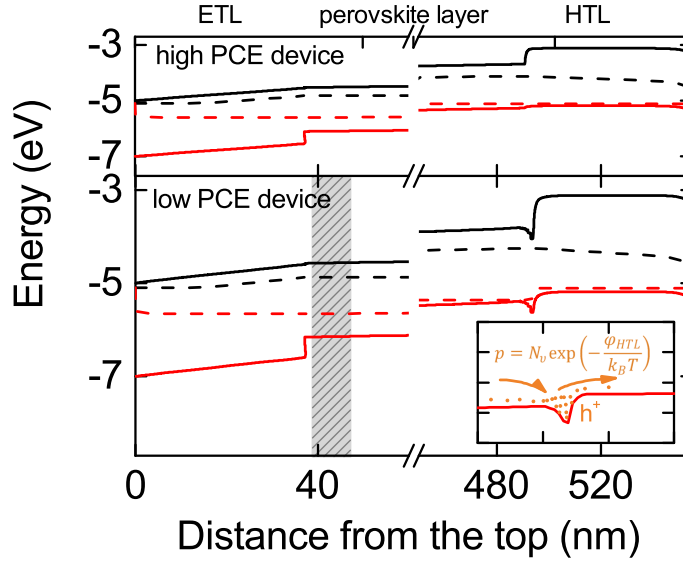


Figure 6: Energy levels of the high (top) and low (bottom) efficiency PSCs. The conduction band (black solid), quasi-Fermi level for electrons (black dashed), and also for holes (red dashed) and valence band (red solid). The inset is to show the band-bending effect on the valence band that takes place for holes.

1 to the recombination process. This explains high losses in V_{oc} which happens
2 due to higher accumulated charge carriers that recombine at high illumination.
3 Both of the following mechanisms are happening simultaneously and explain all
4 the experimental observations.

5 In a short summary, the mechanisms responsible for PCE losses in the de-
6 vice samples prepared using slot-die coating process are twofold. Firstly, part
7 of the FF and V_{oc} are lost due to the increase of defect concentration in the
8 bulk. Meaning, the difference of PCE in the 4×4 cm samples is related to for-
9 mation of bulk defects during the process of sample fabrication. This could be
10 due to the nonuniformity of infrared light irradiation, fabrication time, tem-
11 perature, coating thickness, etc. Since the high PCE device is obtainable,
12 one can resolve nonuniformity issues through more engineering optimization.
13 Secondly, the transportation and interface recombination losses occur at the
14 HTL/perovskite interface for lower PCE samples. These two mechanisms are
15 actually one that occurs at the same time and influences FF and V_{oc} at high
16 light illumination. Clearly, the band-bending leads to lowering of the concentra-
17 tion of free charge carriers and at the same time slows them down at the HTL
18 interface which appears as a charge accumulation. This interface dominating

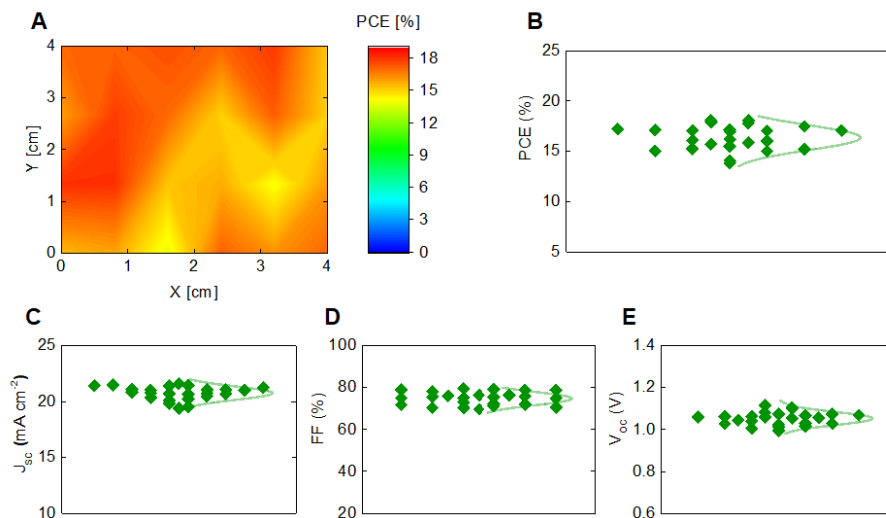


Figure 7: A) Spatial distribution, B) PCE, C) J_{sc} , D) FF, and E) V_{oc} results for the reverse scan measurement perovskite solar cells with TEACl passivation from one 4×4 cm substrate.

1 mechanism is increased with the decreasing quality of the samples. Now, having
 2 the clear point what is influencing the performance of the device prepared with
 3 slot-die coating technique we might create several strategies to improve it.

4 One of the strategies to improve the bulk and interfaces of the perovskite
 5 layer is the passivation technique. Here we applied the 2-thiophene ethylam-
 6 monium chloride (TEACl) dissolved in isopropyl alcohol (IPA) that has been
 7 spin-coated on the top of the absorber layer commonly used in our group [12].
 8 Figure 7A shows spatial distribution of the TEACl passivated PSCs in 4×4 cm
 9 sample. The red and blue color is related to high and low PCE samples, respec-
 10 tively. We clearly see the that upper-left is higher in efficiency. This behavior
 11 has to do most likely with the process of sample preparation. However, it pro-
 12 duces much better-quality sample as compared to the sample without TEACl
 13 passivation. Figure 7B shows the statistical distribution of PCE with an aver-
 14 age efficiency of $16.36 \pm 1.05\%$ for all 24 devices. The lowest and highest PCE
 15 of devices from this substrate are 13.81% and 18.07%, respectively. Figure 7C
 16 shows a very narrow J_{sc} distribution with an average of $20.76 \pm 0.47 \text{ mA cm}^{-2}$.
 17 It clearly shows that optically the samples should not differ much considering all
 18 devices from the same batch. Usually the FF is the most widely distributed PV
 19 parameter that had standard deviation from 4% to almost 6% in the experiment
 20 without using passivation technique. As discussed before, this is the transporta-
 21 tion issues at the HTL interface which are varied from sample to sample. After
 22 applying TEACl, that the FF is improved to an average of $74.79 \pm 2.66\%$ with a

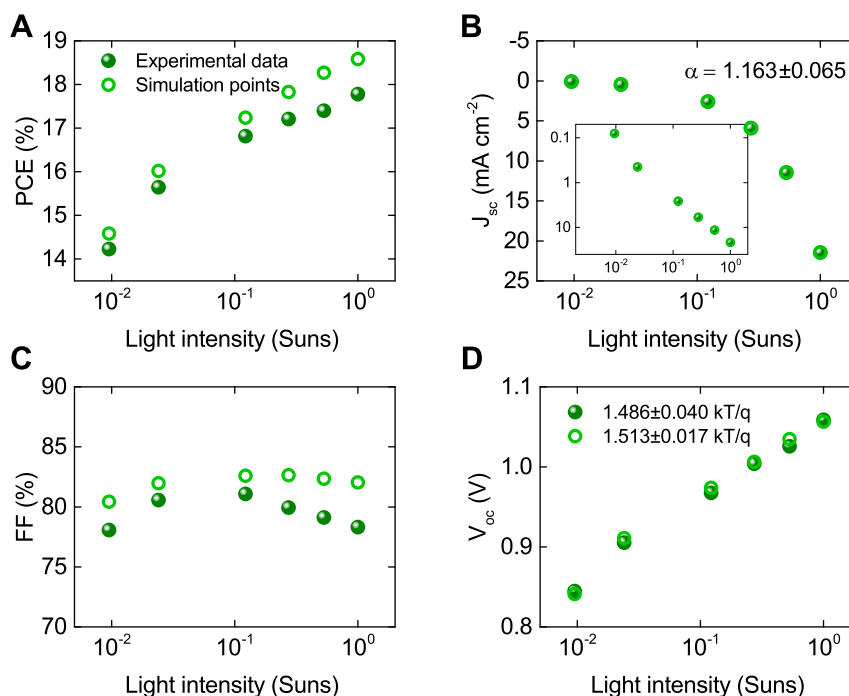


Figure 8: Experimental and simulation results of A) PCE, B) J_{sc} , C) FF, and D) V_{oc} results for the reverse scan measurement of TEACl passivated perovskite solar cells.

1 standard deviation reduced to less than 3% (Figure 7D). The V_{oc} distribution
2 is equal to 1.053 ± 0.025 V which is very close to the devices fabricated without
3 passivation (Figure 7E). This means that probably the defect concentration in
4 the perovskite layer for both bulk and at the interfaces might still vary from
5 sample to sample. All in all, the most visible improvement is in FF which clearly
6 improves the total distribution of PCE of the batch with TEACl passivation.
7 Therefore, the new samples are suffering much less with the aforementioned
8 transportation issues, even for the lowest PCE devices. We examined only one
9 device in detail due to relatively low distribution of all samples and the results
10 are discussed in the following section.

11 Figure S9 (Supplementary Information) shows $J(V)$ experimental and sim-
12 ulated characteristics under modulated light intensities. The goodness-of-fit
13 is equal to 99.51% for all points in the characteristics. The region of SC and
14 OC, and also above matches very well the simulation results, except the MPP
15 has small mismatch at high light intensities. However, for the sample without
16 passivation, we cannot get any better fit. Most likely, the additional mechanism
17 appears at the ETL interface once passivating the samples with TEACl layer.

18 Figure 8 shows the experimental and simulation results of PV parameters

1 for the TEACl passivated sample. The PCE of the representative device goes
 2 linearly with light intensity. The maximum point is reached at 1 sun (Figure 8A)
 3 showing very similar tendency to high PCE sample without passivation layer
 4 (Figure 2A). J_{sc} is in a linear function of modulated light intensity with an alpha
 5 factor of 1.136 ± 0.065 . Thus, it is the highest values among all samples without
 6 or with TEACl. We have noticed that the light intensity at 0.01 suns have
 7 the highest error here which clearly influence this value and its measurement
 8 precision. However, it is still very close to 1 so the nonradiative recombination
 9 dominates the losses (Figure 8B). Figure 8C shows the FF in a function of
 10 light intensity. It is very similar to that of high efficiency PSC without TEACl
 11 passivation. Very flat curve with peak-FF at 0.1 suns has reached 81.07% which
 12 is around 1% higher if comparing to high efficiency PSC. The result indicates
 13 the recombination of bulk defects recombination is slightly reduced by TEACl
 14 passivation. A small drop toward higher light intensity is observed and it reaches
 15 78.32% at one sun. We did further analysis to determine the interface is more
 16 dominated by the transport loss or recombination process. Figure 8D shows
 17 V_{oc} as a function of modulated light intensity. At 1 sun, V_{oc} is equal to 1.059 V
 18 which shows 10 mV improvement as compared to the high efficiency PSC without
 19 TEACl passivation. It is rather negligible improvement within the statistical
 20 error. Also, the ideality factor is equal to 1.486 ± 0.040 kT/q which is very close
 21 to the reference solar cell. Meaning, the dominant recombination mechanism
 22 has not changed and the ratio between interface and bulk defect recombination
 23 is still very close to be the same. Thus, the observed losses at 1 sun are more
 24 likely related to the transportation at the interface which has not been observed
 25 in the previous samples without TEACl passivation.

26 In the electrical modeling we used the same structure and fixed parameters
 27 as in the PSCs without TEACl passivation. From the simulation results, we
 28 can see very small drop of bulk defect concentration that is equal to 1.08 ± 10^{22}
 29 m^{-3} . It means that the traps in the bulk have been reduced by 7% if comparing
 30 to the reference PSC. At the same time, we found the reduction of HTL in-
 31 terface defects to $41.25 \pm 10^{14} m^{-2}$ which is again improvement of around 18%.
 32 However, the trap concentration at the ETL interface is higher than that in
 33 the reference PSC and it is equal to $50.41 \pm 10^{14} m^{-2}$. This means that the
 34 increase of 61% of defect density at this interface. We did not find any HTL
 35 band-bending here. However, the lack of match of experimental FF at high light
 36 intensity to simulation results might suggest an additional transport mechanism
 37 at the perovskite/ETL interface. The other argument is the increase of interface
 38 recombination at this side which might be a result of interaction with TEACl.

39 In our previous work, we demonstrated that anionic and cationic defect in
 40 perovskite can be passivated by Cl^- and TEA^+ respectively [12]. For the Cl^-
 41 anion, it can diffuse into perovskite film to compensate the anion defect of halide
 42 vacancy (example: I^- vacancy) because of its small atom size and strong bonding
 43 with Pb atom. That is why we can see the trap of bulk and HTL interface could
 44 be reduced. On the other hand, the large-sized TEA^+ cation can only stay in
 45 the surface and form a 2D perovskite thin layer on top of the 3D perovskite film.
 46 In comparison of 3D perovskite, the 2D perovskite exhibits a wider band gap,



1 which changes the band alignment of ETL interface and thus enhances the V_{oc}
 2 of perovskite solar cell [36, 37]. However, if this 2D perovskite layer is too thick,
 3 it could be also a charge transport barrier because of its low charge transport
 4 properties [38, 39]. Therefore, the preparation of this 2D layer should be well
 5 designed and controlled to improve the performance of the perovskite solar cell.
 6 From the performance of the passivated device, we cannot see the significant
 7 improvement in V_{oc} . Also, from the result of the drift-diffusion analysis, we
 8 could see that the additional interface transportation mechanism might appear
 9 at the ETL side. It means that the 2D layer might not be fully converted or
 10 not well-prepared in this study. However, this would be the topic of another
 11 studies. All in all, the champion samples with TEACl passivation are showing
 12 small improvements on the bulk and HTL/perovskite interface but at the same
 13 time small reduction of perovskite/ETL interface quality. It does not lead to
 14 extraordinary improvement of the PCE of the devices which is only around 0.5%
 15 for the champion PSCs. However, most importantly the passivation technique
 16 has improved the statistical efficiency of the devices and drastically reduced the
 17 amount of low PCE samples.

18 3 Conclusions

19 We report the PSCs prepared using slot-die coating process with the rapid near
 20 infrared heating technique in ambient air. The results show very wide distribu-
 21 tion of efficiency of all device samples in statistical and spatial distributions for
 22 three batches. The difference in PCE from sample to sample has been mostly
 23 related to FF and V_{oc} suggesting that the effect comes from the electrical losses.
 24 The Shockley-Queisser model was used to do loss analysis. The major distribu-
 25 tion to the PCE for all samples is coming from electrical mechanisms related to
 26 nonradiative and transportation losses. The drift-diffusion modeling was used to
 27 determine the dominating mechanisms responsible for the electrical losses using
 28 high PCE sample as a reference one. The bulk defect density is shown to be lin-
 29 early changing with the quality of the PSCs. The defects at the HTL/perovskite
 30 interface are resulted in the Fermi level pinning which is observed in the lower
 31 quality samples. The transportation mechanism is dominated in this situation
 32 due to the high accumulation of charge carriers at the interface, and there-
 33 fore high interface defect recombination. Finding the dominant loss channels
 34 in the PSCs have made a clear strategy to improve the performance of devices.
 35 Both of the dominant mechanisms of losses have been reduced by passivation
 36 technique using TEACl material. It leads to the improvement of the bulk and
 37 HTL/perovskite interface of the champion device. However, higher losses are
 38 observed at the ETL side which was not accounted in the previous devices.
 39 This results in small improvement of PCE performance but huge improvement
 40 of PCE distribution in the same batch of PSCs.



4 Experimental Section

Preparation of solutions for device fabrication: In ambient condition (25–30°C, 40–60% RH), 0.25 M nickel acetate tetrahydrate ($\text{Ni}(\text{CH}_3\text{COO})_2 \cdot 4 \text{H}_2\text{O}$, 99.0%, SHOWA Chemical) was dissolved in ethanol (anhydrous, Fisher Chemical) to prepare a NiOx precursor solution. The solution was then stirred at 60°C until it became transparent. After adding 1 molar equivalent of ethanolamine (99%, ACROS Organic), the solution was filtered with 0.22 μm poly(1,1,2,2-tetrafluoroethylene) (PTFE). The poly [3-(6-carboxyhexyl)thiophene-2,5-diyl] (P3HT–COOH, regioregular, Rieke metals) was dissolved in dimethylformamide (DMF, anhydrous, ACROS Organic) with a concentration of 0.125 mg mL^{-1} . The following three solutions were prepared in a N_2 glove box, 4 h before using them. 0.4M perovskite ($\text{Cs}_{0.2}\text{FA}_{0.8}\text{Pb}(\text{I}_{0.93}\text{Br}_{0.07})_3$) precursor solution: 184 mg lead iodide (PbI_2 , 99.99985%, Alfa Aesar), 55 mg formamidinium iodide (FAI, STAREK scientific Co. Ltd.), 17 mg cesium bromide (CsBr , 99%, Alfa Aesar) and 0.02 mg polyethylene glycol (PEG, Mw 6k, ACROS Organic) were dissolved in a solvent mixture of γ -butyrolactone (GBL, 99+%, ACROS Organic), n-butanol (99%, ACROS Organic) and dimethyl sulfoxide (DMSO, 99.7+%, ACROS Organic) at volume ratio of 1:1:8. 2-Thiophene ethylammonium chloride (TEACl) was prepared according to literature [12]. Then, TEACl was dissolved in isopropanol (IPA, 99.5%, ACROS Organic) at a concentration of 4 mM. The phenyl-C61-butyric acid methyl ester (PCBM, 99.5%, Solenne B.V.) was used as the electron transporting layer (ETL) with a concentration of 20 mg mL^{-1} in chlorobenzene (CB, 99+%, ACROS Organic). The concentration of 0.1 wt% of polyethyleneimine (PEI, branched, Average Mn 10k, Sigma-Aldrich) was prepared in isopropyl alcohol to process as a work functional modifier layer (WFL)

Device fabrication for perovskite solar cell: The slot-die coating was carried out in ambient air at 30°C and with relative humidity 45–55%. First, the fluorine doped tin oxide (FTO), 4×4 cm, coated glass substrates (TEC7, Hartford) were washed by ultrasonic bath for 15 minutes using detergent solution, methanol and isopropanol, respectively. The substrates were blown dry with nitrogen, then treated with UV-Ozone for 15 min. For parameters of slot-die coating, the height of the upstream and downstream lips was in the range of 170 μm – 200 μm for the slot-die head, which contains a 100 μm shim inside the die. The wet film of NiOx precursor solution was controlled at the substrate temperature of 55°C, coating speed of 0.5 m min^{-1} and the feeding rate of 2.5 mL min^{-1} . Then crystalline film of NiOx was annealed at 300°C for 5 min. Then P3HT–COOH solution was controlled at the substrate temperature of 95°C, coating speed of 1.5 m min^{-1} and the feeding rate of 1.5 mL min^{-1} . The P3HT–COOH film was annealed at 140°C for 10 min. The wet film of perovskite precursor solution was applied on top of NiOx/P3HT–COOH film at a coating speed of 1.0 m min^{-1} and the feeding rate of 2.0 mL min^{-1} . The wet film was dried and crystallized by passing through the 15 kW NIR at 1.8 m min^{-1} . For passivation layer, the TEACl solution was spin-coated at 3000 rpm for 20 s onto the perovskite layer and then thermally annealed at 70°C for 15 min.



1 The spin coating process of ETL and WFL on large area film containing
2 HTL and perovskite layer was also used initially to fabricate the solar cell. The
3 4×4 cm slot-die coated film were cut to 2×2 cm of substrate size before the
4 deposition of PCBM and PEI layer. Then, the $50 \mu\text{L}$ of PCBM solution and
5 $50 \mu\text{L}$ of PEI solution were spin-coated on the film at 1000 rpm for 30 s and
6 3000 rpm for 30 s, respectively in nitrogen. Then, 100 nm of silver electrodes
7 was deposited on the top of WF layer with an active area of 0.09 cm^2 by using
8 thermal evaporation. The large area film has been prepared on the transparent
9 electrode using a slot-die machine (Easycoater, Coatema). Spin-coated layers
10 were prepared using spin-coater (WS-400B 6NPP, Laurell Technologies).

11 Measurement techniques: The current—voltage curves of devices were mea-
12 sured by using a source meter (Keithley 2410) with 100 mW cm^{-2} illumination
13 of AM1.5G solar simulator (YSS-150A, Yamashita Denso). The neutral den-
14 sity (ND) filters (Thorlabs) have been placed directly on the light path from
15 the light source to the sample. The thickness of coating was measured using
16 profilometer (Dektak 150, Veeco). The cross-section image was made using
17 SEM (S3000N, Hitachi). EQE curves of devices were measured by using a EQE
18 system (LSQE-R, LiveStrong Optoelectronics).

19 5 Simulation Section

20 For the simulation of the PSCs, our drift--diffusion software was used [22].
21 The two-step fitting procedure has been used to match the experimental data.
22 Firstly, the global minimum is searched using the differential evolution algorithm
23 [40]. Secondly, the Nelder-Mead model [41, 42] is applied to further optimize.
24 In order to define the goodness-of-fit the Chi-Square test has been used. The
25 goodness-of-fit is referring to R^2 value from the regression analysis. Therefore,
26 the value is in the range of 0% to 100%, depending on how well the simulation
27 data match the experimental results. Table 1 shows all the parameters used for
28 the simulation of PSCs. The trap densities in the bulk and at the interface of the
29 absorber layer, and also band-bending parameters are all shown in Table 1(b).
30 The values are different for high, intermediate and low PCE samples. Here, we
31 considered only steady-state conditions and did not study the dynamical effect
32 of ions which results in hysteresis. We show that ions in steady-state conditions
33 affect the operation of solar cell negligibly [35]. The generation profile was
34 calculated using the optical transfer-matrix model [43, 44]. It was calculated
35 using the optical real and imaginary refractive index in a function of wavelength
36 for NiOx, perovskite and PCBM measured experimentally.

37 The electrical parameters are adopted from the literature or from the fitting
38 process. For the hole transporting layer (HTL), NiOx was used and part of
39 the electrical parameters were adopted from the literature [24, 29, 45, 46]. Per-
40 ovskite material was defined as an active layer with electrical parameters taken
41 from the literature [23, 26, 27, 28] or from fitting to the experimental data
42 [20, 30]. For the electron transporting layer (ETL), we used PCBM material
43 with electrical parameters adopted from the literature [28, 25, 47, 48, 49].



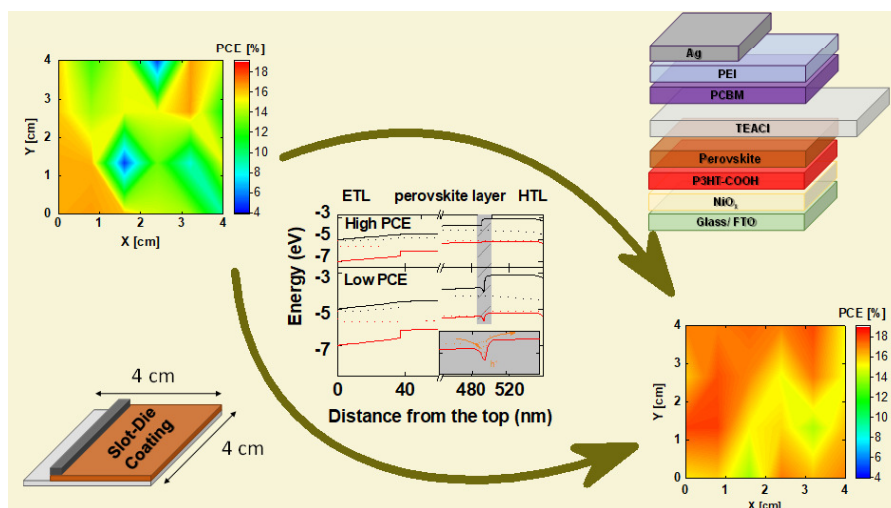


Figure 9: TOC graphics

6 Acknowledgment

This research was funded in part by National Science Centre, in cooperation with the M-ERA.NET 3 Call 2021 for the grant number 2021/03/Y/ST5/00233. This project has received funding from the European Union's Horizon 2020 research and innovation program under grant agreement No 958174. Calculations were carried out at the Academic Computer Centre (CI TASK) in Gdansk. National Science and Technology of Taiwan provides fund for this research under the grant number of 111-2923-E-002-012-MY3.

7 Keywords

perovskite solar cells, photovoltaics, slot-die coating, upscaling, interface

8 Supplementary Information

Supplementary Information: additional figures for the manuscript

9 TOC

References

- [1] Abdulaziz S. R. Bati, Yu Lin Zhong, Paul L. Burn, Mohammad Khaja Nazeeruddin, Paul E. Shaw, and Munkhbayar Batmunkh. Next-generation

- 1 applications for integrated perovskite solar cells. *Commun Mater*, 4(2),
2 2023.
- 3 [2] Jaeki Jeong, Minjin Kim, Jongdeuk Seo, Haizhou Lu, Paramvir Ahlawat,
4 Aditya Mishra, Yingguo Yang, Michael A. Hope, Felix T. Eickemeyer,
5 Maengsuk Kim, In Woo Choi Yung Jin Yoon, Barbara Primera Darwich,
6 Seung Ju Choi, Yimhyun Jo, Jun Hee Lee, Bright Walker, Shaik M.
7 Zakeeruddin, Lyndon Emsley, Ursula Rothlisberger, Anders Hagfeldt,
8 Dong Suk Kim, and Michael Gratzel. Pseudo-halide anion engineering
9 for α -fapbi₃ perovskite solar cells, 2021.
- 10 [3] Yulia Galagan. Perovskite solar cells from lab to fab: the main challenges to
11 access the market. *Oxford Open Materials Science*, 1(1), 12 2020. itaa007.
- 12 [4] Zhibin Yang, Chu-Chen Chueh, Fan Zuo, Jong H. Kim, Po-Wei Liang, and
13 Alex K.-Y. Jen. High-performance fully printable perovskite solar cells via
14 blade-coating technique under the ambient condition. *Advanced Energy*
15 *Materials*, 5(13):1500328, 2015.
- 16 [5] Sampson Adjokatse, Hong-Hua Fang, Herman Duim, and Maria Antonietta
17 Loi. Scalable fabrication of high-quality crystalline and stable fapbi₃ thin
18 films by combining doctor-blade coating and the cation exchange reaction.
19 *Nanoscale*, 11:5989–5997, 2019.
- 20 [6] Shih-Han Huang, Kuo-Yu Tian, Hung-Che Huang, Chia-Feng Li, Wei-
21 Cheng Chu, Kun-Mu Lee, Yu-Ching Huang, and Wei-Fang Su. Control-
22 ling the morphology and interface of the perovskite layer for scalable high-
23 efficiency solar cells fabricated using green solvents and blade coating in an
24 ambient environment. *ACS Applied Materials & Interfaces*, 12(23):26041–
25 26049, 2020. PMID: 32434322.
- 26 [7] James E. Bishop, Thomas J. Routledge, and David G. Lidzey. Advances
27 in spray-cast perovskite solar cells. *The Journal of Physical Chemistry*
28 *Letters*, 9(8):1977–1984, 2018. PMID: 29608061.
- 29 [8] Rahul Patidar, Daniel Burkitt, Katherine Hooper, David Richards, and
30 Trystan Watson. Slot-die coating of perovskite solar cells: An overview.
31 *Materials Today Communications*, 22:100808, 2020.
- 32 [9] Xiaoyu Ding, Jianhua Liu, and Tequila A. L. Harris. A review of the
33 operating limits in slot die coating processes. *AIChE Journal*, 62(7):2508–
34 2524, 2016.
- 35 [10] Shih-Han Huang, Cheng-Kang Guan, Pei-Huan Lee, Hung-Che Huang,
36 Chia-Feng Li, Yu-Ching Huang, and Wei-Fang Su. Toward all slot-die
37 fabricated high efficiency large area perovskite solar cell using rapid near in-
38frared heating in ambient air. *Advanced Energy Materials*, 10(37):2001567,
39 2020.

- 1 [11] Amalraj Peter Amalathas, Lucie Landová, Zdeňka Hájková, Lukáš Horák,
2 Martin Ledinsky, and Jakub Holovský. Controlled growth of large grains in
3 $\text{CH}_3\text{NH}_3\text{PbI}_3$ perovskite films mediated by an intermediate liquid phase with-
4 out an antisolvent for efficient solar cells. *ACS Applied Energy Materials*,
5 3(12):12484–12493, 2020.
- 6 [12] Kai-Chi Hsiao, Meng-Huan Jao, Bo-Ting Li, Ting-Han Lin, Stan Hsueh-
7 Chung Liao, Ming-Chung Wu, and Wei-Fang Su. Enhancing efficiency and
8 stability of hot casting p-i-n perovskite solar cell via dipolar ion passiva-
9 tion. *ACS Applied Energy Materials*, 2(7):4821–4832, 2019.
- 10 [13] Mark V. Khenkin, Eugene A. Katz, Antonio Abate, Giorgio Bardizza,
11 Joseph J. Berry, Christoph Brabec, Francesca Brunetti, Vladimir Bulović,
12 Quinn Burlingame, Aldo Di Carlo, Rongrong Cheacharoen, Yi-Bing Cheng,
13 Alexander Colmann, Stephane Cros, Konrad Domanski, Michał Dusza,
14 Christopher J. Fell, Stephen R. Forrest, Yulia Galagan, Diego Di Girolamo,
15 Michael Grätzel, Anders Hagfeldt, Elizabeth von Hauff, Harald Hoppe, Jeff
16 Kettle, Hans Köbler, Marina S. Leite, Shengzhong (Frank) Liu, Yueh-Lin
17 Loo, Joseph M. Luther, Chang-Qi Ma, Morten Madsen, Matthieu Manceau,
18 Muriel Matheron, Michael McGehee, Rico Meitzner, Mohammad Khaja
19 Nazeeruddin, Ana Flavia Nogueira, Çağla Odabaşı, Anna Osherov, Nam-
20 Gyu Park, Matthew O. Reese, Francesca De Rossi, Michael Saliba, Ulrich S.
21 Schubert, Henry J. Snaith, Samuel D. Stranks, Wolfgang Tress, Pavel A.
22 Troshin, Vida Turkovic, Sjoerd Veenstra, Iris Visoly-Fisher, Aron Walsh,
23 Trystan Watson, Haibing Xie, Ramazan Yıldırım, Shaik Mohammed Za-
24 keeruddin, Kai Zhu, and Monica Lira-Cantu. Consensus statement for
25 stability assessment and reporting for perovskite photovoltaics based on
26 isos procedures. *Nature Energy*, 5(1):35–49, Jan 2020.
- 27 [14] J.C. Wang, X.C. Ren, S.Q. Shi, C.W. Leung, and Paddy K.L. Chan. Charge
28 accumulation induced s-shape j-v curves in bilayer heterojunction organic
29 solar cells. *Organic Electronics*, 12(6):880–885, 2011.
- 30 [15] M. Prete, M. V. Khenkin, D. Glowienka, B. R. Patil, J. S. Lissau, I. Do-
31 gan, J. L. Hansen, T. Leißner, J. Fiutowski, H.-G. Rubahn, B. Julsgaard,
32 P. Balling, V. Turkovic, Y. Galagan, E. A. Katz, and M. Madsen. Bias-
33 dependent dynamics of degradation and recovery in perovskite solar cells.
34 *ACS Applied Energy Materials*, 4(7):6562–6573, 2021.
- 35 [16] Lisa Krückemeier, Uwe Rau, Martin Stoltterfoht, and Thomas Kirchartz.
36 How to report record open-circuit voltages in lead-halide perovskite solar
37 cells. *Advanced Energy Materials*, 10(1):1902573, 2020.
- 38 [17] Jean-Francois Guillemoles, Thomas Kirchartz, David Cahen, and Uwe Rau.
39 Guide for the perplexed to the shockley–queisser model for solar cells. *Na-
40 ture Photonics*, 13(8):501–505, Aug 2019.

- 1 [18] Jiantuo Gan, Robert L.Z. Hoyer, Yulia Ievskaya, Lasse Vines, Andrew T.
2 Marin, Judith L. MacManus-Driscoll, and Edouard V. Monakhov. Elu-
3 cidating the origin of external quantum efficiency losses in cuprous oxide
4 solar cells through defect analysis. *Solar Energy Materials and Solar Cells*,
5 209:110418, 2020.
- 6 [19] Damian Glowienka and Yulia Galagan. Light intensity analysis of pho-
7 tovoltaic parameters for perovskite solar cells. *Advanced Materials*,
8 34(2):2105920, 2022.
- 9 [20] Damian Glowienka, Francesco Di Giacomo, Mehrdad Najafi, Ilker Dogan,
10 Alfredo Mameli, Fallon J. M. Colberts, Jędrzej Szmytkowski, and Yulia
11 Galagan. Effect of different bromine sources on the dual cation mixed
12 halide perovskite solar cells. *ACS Applied Energy Materials*, 3(9):8285–
13 8294, 2020.
- 14 [21] Weijian Wang, Gang Yu, and Sanam Attique. Dragon mimic shape facili-
15 tate ultrahigh-performance flexible all-perovskite tandem solar cells. *Solar*
16 *RRL*, n/a(n/a):2201064, 2023.
- 17 [22] Damian Glowienka, Dong Zhang, Francesco Di Giacomo, Mehrdad Najafi,
18 Sjoerd Veenstra, Jędrzej Szmytkowski, and Yulia Galagan. Role of surface
19 recombination in perovskite solar cells at the interface of htl/ch3nh3pb3.
20 *Nano Energy*, 67:104186, 2020.
- 21 [23] Federico Brivio, Keith T. Butler, Aron Walsh, and Mark van Schilf-
22 gaarde. Relativistic quasiparticle self-consistent electronic structure of hy-
23 brid halide perovskite photovoltaic absorbers. *Phys. Rev. B*, 89:155204,
24 Apr 2014.
- 25 [24] Qiqi He, Kai Yao, Xiaofeng Wang, Xuefeng Xia, Shifeng Leng, and Fan
26 Li. Room-temperature and solution-processable cu-doped nickel oxide
27 nanoparticles for efficient hole-transport layers of flexible large-area per-
28 ovskite solar cells. *ACS Applied Materials & Interfaces*, 9(48):41887–41897,
29 2017.
- 30 [25] Germà Garcia-Belmonte, Antoni Munar, Eva M. Barea, Juan Bisquert,
31 Irati Ugarte, and Roberto Pacios. Charge carrier mobility and lifetime of
32 organic bulk heterojunctions analyzed by impedance spectroscopy. *Organic*
33 *Electronics*, 9(5):847 – 851, 2008.
- 34 [26] Rebecca L. Milot, Giles E. Eperon, Henry J. Snaith, Michael B. John-
35 ston, and Laura M. Herz. Temperature-dependent charge-carrier dynam-
36 ics in ch3nh3pb3 perovskite thin films. *Advanced Functional Materials*,
37 25(39):6218–6227, 2015.
- 38 [27] Xu Sun, Chunfu Zhang, Jingjing Chang, Haifeng Yang, He Xi, Gang Lu,
39 Dazheng Chen, Zhenhua Lin, Xiaoli Lu, Jincheng Zhang, and Yue Hao.
40 Mixed-solvent-vapor annealing of perovskite for photovoltaic device effi-
41 ciency enhancement. *Nano Energy*, 28:417–425, 2016.



- 1 [28] Tejas S. Sherkar, Cristina Momblona, Lidón Gil-Escrig, Henk J. Bolink,
2 and L. Jan Anton Koster. Improving perovskite solar cells: Insights from a
3 validated device model. *Advanced Energy Materials*, 7(13):1602432, 2017.
- 4 [29] Gayatri Natu, Panitat Hasin, Zhongjie Huang, Zhiqiang Ji, Mingfu He, and
5 Yiyang Wu. Valence band-edge engineering of nickel oxide nanoparticles
6 via cobalt doping for application in p-type dye-sensitized solar cells. *ACS*
7 *Applied Materials & Interfaces*, 4(11):5922–5929, 2012. PMID: 23054373.
- 8 [30] Jędrzej Szmytkowski, Yulia Galagan, and Damian Glowienka. Exploring
9 the interfacial effects at the etl/perovskite boundary in the semitransparent
10 perovskite solar cells. *Solar Energy*, 266:112176, 2023.
- 11 [31] Bekir Turedi, Muhammad N. Lintangpradipto, Oskar J. Sandberg, Aren
12 Yazmaciyan, Gebhard J. Matt, Abdullah Y. Alsalloum, Khulud Almasabi,
13 Kostiantyn Sakhatskyi, Sergii Yakunin, Xiaopeng Zheng, Rounak Naphade,
14 Saidkhodzha Nematullov, Vishal Yeddu, Derya Baran, Ardalan Armin,
15 Makhsud I. Saidaminov, Maksym V. Kovalenko, Omar F. Mohammed, and
16 Osman M. Bakr. Single-crystal perovskite solar cells exhibit close to half a
17 millimeter electron-diffusion length. *Advanced Materials*, 34(47):2202390,
18 2022.
- 19 [32] Thibaut Gallet, David Grabowski, Thomas Kirchartz, and Alex
20 Redinger. Fermi-level pinning in methylammonium lead iodide perovskites.
21 *Nanoscale*, 11:16828–16836, 2019.
- 22 [33] Sebastian Wilken, Jürgen Parisi, and Holger Borchert. Role of oxygen
23 adsorption in nanocrystalline zno interfacial layers for polymer–fullerene
24 bulk heterojunction solar cells. *The Journal of Physical Chemistry C*,
25 118(34):19672–19682, 2014.
- 26 [34] Wolfgang Tress, Mozhgan Yavari, Konrad Domanski, Pankaj Yadav, Bjoern
27 Niesen, Juan Pablo Correa Baena, Anders Hagfeldt, and Michael Graetzel.
28 Interpretation and evolution of open-circuit voltage, recombination, ide-
29 ality factor and subgap defect states during reversible light-soaking and
30 irreversible degradation of perovskite solar cells. *Energy Environ. Sci.*,
31 11:151–165, 2018.
- 32 [35] Damian Glowienka and Jędrzej Szmytkowski. Numerical modeling of ex-
33 citon impact in two crystallographic phases of the organo-lead halide per-
34 ovskite (ch₃nh₃pbi₃) solar cell. *Semiconductor Science and Technology*,
35 34(3):035018, feb 2019.
- 36 [36] Albertus A. Sutanto, Pietro Caprioglio, Nikita Drigo, Yvonne J. Hof-
37 stetter, Ines Garcia-Benito, Valentin I.E. Queloz, Dieter Neher, Moham-
38 mad Khaja Nazeeruddin, Martin Stollerfoht, Yana Vaynzof, and Giulia
39 Grancini. 2d/3d perovskite engineering eliminates interfacial recombina-
40 tion losses in hybrid perovskite solar cells. *Chem*, 7(7):1903–1916, 2021.



- 1 [37] Guangbao Wu, Rui Liang, Mingzheng Ge, Guoxing Sun, Yuan Zhang, and
2 Guichuan Xing. Surface passivation using 2d perovskites toward efficient
3 and stable perovskite solar cells. *Advanced Materials*, 34(8):2105635, 2022.
- 4 [38] Liguao Gao, Fei Zhang, Xihan Chen, Chuanxiao Xiao, Bryon W. Lar-
5 son, Sean P. Dunfield, Joseph J. Berry, and Kai Zhu. Enhanced charge
6 transport by incorporating formamidinium and cesium cations into two-
7 dimensional perovskite solar cells. *Angewandte Chemie International Edi-
8 tion*, 58(34):11737–11741, 2019.
- 9 [39] Jiselle Y. Ye, Jinhui Tong, Jun Hu, Chuanxiao Xiao, Haipeng Lu, Sean P.
10 Dunfield, Dong Hoe Kim, Xihan Chen, Bryon W. Larson, Ji Hao, Kang
11 Wang, Qian Zhao, Zheng Chen, Huamin Hu, Wei You, Joseph J. Berry,
12 Fei Zhang, and Kai Zhu. Enhancing charge transport of 2d perovskite
13 passivation agent for wide-bandgap perovskite solar cells beyond 21%. *Solar
14 RRL*, 4(6):2000082, 2020.
- 15 [40] Manolis Georgioudakis and Vagelis Plevris. A comparative study of differ-
16 ential evolution variants in constrained structural optimization. *Frontiers
17 in Built Environment*, 6:102, 2020.
- 18 [41] J. A. Nelder and R. Mead. A Simplex Method for Function Minimization.
19 *The Computer Journal*, 7(4):308–313, 01 1965.
- 20 [42] Matthew Newville, Till Stensitzki, Daniel B. Allen, Michal Rawlik, An-
21 tonino Ingargiola, and Andrew Nelson. Lmfit: Non-Linear Least-Square
22 Minimization and Curve-Fitting for Python, June 2016.
- 23 [43] Leif A. A. Pettersson, Lucimara S. Roman, and Olle Inganäs. Modeling
24 photocurrent action spectra of photovoltaic devices based on organic thin
25 films. *Journal of Applied Physics*, 86(1):487–496, 1999.
- 26 [44] George F. Burkhard, Eric T. Hoke, and Michael D. McGehee. Account-
27 ing for interference, scattering, and electrode absorption to make accurate
28 internal quantum efficiency measurements in organic and other thin solar
29 cells. *Advanced Materials*, 22(30):3293–3297, 2010.
- 30 [45] A. Castro-Carranza, J. C. Nolasco, M. Estrada, R. Gwoziecki, M. Ben-
31 wadih, Y. Xu, A. Cerdeira, L. F. Marsal, G. Ghibaudo, B. Iniguez, and
32 J. Pallares. Effect of density of states on mobility in small-molecule n-type
33 organic thin-film transistors based on a perylene diimide. *IEEE Electron
34 Device Letters*, 33(8):1201–1203, 2012.
- 35 [46] Naoto Tsutsumi, Kenji Kinashi, Kento Masumura, and Kenji Kono. Pho-
36 torefractive performance of poly(triarylamine)-based polymer composites:
37 An approach from the photoconductive properties. *Journal of Polymer
38 Science Part B: Polymer Physics*, 53(7):502–508, 2015.



- 1 [47] Roderick C. I. MacKenzie, Thomas Kirchartz, George F. A. Dibb, and
2 Jenny Nelson. Modeling nongeminate recombination in p3ht:pcbm solar
3 cells. *The Journal of Physical Chemistry C*, 115(19):9806–9813, 2011.
- 4 [48] Dhruva B. Khadka, Yasuhiro Shirai, Masatoshi Yanagida, James W. Ryan,
5 and Kenjiro Miyano. Exploring the effects of interfacial carrier transport
6 layers on device performance and optoelectronic properties of planar per-
7 ovskite solar cells. *J. Mater. Chem. C*, 5:8819–8827, 2017.
- 8 [49] G. Juška, K. Genevičius, N. Nekrašas, G. Sliauzys, and G. Dennler. Tri-
9 molecular recombination in polythiophene: fullerene bulk heterojunction
10 solar cells. *Applied Physics Letters*, 93(14):143303, 2008.